scientific reports

Check for updates

OPEN

Designing a multi-epitope vaccine against Pseudomonas aeruginosa via integrating reverse vaccinology with immunoinformatics approaches

Fei Zhu[1,2,3,4,5,7,8], Rongliu Qin[1,2,3,4,5,7,8], Shiyang Ma[1,2,3,4,5,7], Ziyou Zhou[1,2,3,4,5,7], Caixia Tan[5,6], Hang Yang[1,2,3,4,5,7], Peipei Zhang[1,2,3,4,5,7], Yizhong Xu[1,2,3,4,5,7], Yuying Luo[1,2,3,4,5,7], Jie Chen[1,2,3,4,5,7]✉ & Pinhua Pan[1,2,3,4,5,7]✉

Pseudomonas aeruginosa **is a typically opportunistic pathogen responsible for a wide range of nosocomial infections. In this study, we designed two multi-epitope vaccines targeting *P. aeruginosa* proteins, incorporating cytotoxic T lymphocyte (CTL), helper T lymphocyte (HTL), and linear B lymphocyte (LBL) epitopes identified using reverse vaccinology and immunoinformatics approaches. The vaccines exhibited favorable physicochemical properties, including stability, solubility, and optimal molecular weight, suggesting their potential as viable candidates for vaccine development. Molecular docking studies revealed strong binding affinity to Toll-like receptors 1 (TLR1) and 2 (TLR2). Furthermore, molecular dynamics simulations confirmed the stability of the vaccine-TLR complexes over time. Immune simulation analyses indicated that the vaccines could induce robust humoral and cellular immune responses, providing a promising new approach for combating *P. aeruginosa* infections, particularly in the face of increasing antibiotic resistance.**

Keywords *Pseudomonas aeruginosa*, Multi-epitope vaccine, Molecular docking, Molecular dynamics simulation, Reverse vaccinology, Immunoinformatics

An opportunist pathogen, *Pseudomonas aeruginosa* (*P. aeruginosa*) is a bacterial Gram-negative species from the *Pseudomonadaceae* family[1]. *P. aeruginosa* infection primarily affects individuals with malfunctioning respiratory tracts or compromised immune systems, such as ventilator-associated pneumonia, COPD, CF, and bronchiectasis[2–5]. Moreover, *P. aeruginosa*is associated with infections of the skin and soft tissues, bacteremia, urinary tract infections, and gastrointestinal infections. Other infections are particularly prevalent among those with severe burns, cancer, or AIDS[1].

As an opportunistic organism responsible for nosocomial infections, the prevalence of *P. aeruginosa* infections has increased over the past decade, with current estimates suggesting they account for 7.1–7.3% of all healthcare-associated infections[6]. Research has shown that individuals with COPD who are receiving inhaled corticosteroid therapy face a significantly increased risk of *Pseudomonas aeruginosa* infection, with the risk escalating in proportion to the dosage[7]. Furthermore, *P. aeruginosa* poses a substantial concern to public health, particularly in intensive care units and long-term acute care hospitals where it significantly increases morbidity and mortality, as illustrated by the evolution of antimicrobial resistance[6]. According to epidemiological data, approximately 700,000 individuals succumb to antibiotic-resistant bacterial infections annually[8]. Due to their

[1]Department of Respiratory Medicine, National Key Clinical Specialty, Branch of National Clinical Research Center for Respiratory Disease, Xiangya Hospital, Central South University, Changsha, Hunan, China. [2]Center of Respiratory Medicine, Xiangya Hospital, Central South University, Changsha, Hunan, China. [3]Clinical Research Center for Respiratory Diseases in Hunan Province, Changsha, Hunan, China. [4]Hunan Engineering Research Center for Intelligent Diagnosis and Treatment of Respiratory Disease, Changsha, Hunan, China. [5]National Clinical Research Center for Geriatric Disorders, Xiangya Hospital, Changsha, Hunan, China. [6]Department of Infection Control Center of Xiangya Hospital, Central South University, Changsha, Hunan, China. [7]FuRong Laboratory, Changsha 410008, Hunan, China. [8]These authors contributed equally to this work. ✉email: chenjie869@csu.edu.cn; pinhuapan668@csu.edu.cn

versatility and adaptability, bacteria have developed both inherent and acquired mechanisms of resistance to multiple antibiotics. One such mechanism is the emergence of multidrug-resistant (MDR) clones, which greatly diminish the efficacy of treatments[9]. Therefore, a post-antibiotic era is imminent given the rising incidence of MDR infections and the dearth of new pharmaceutical discoveries[10]. This highlights the urgent requirement to explore innovative and practical alternative strategies.

Recent research has explored numerous vaccine strategies targeting *P. aeruginosa*. Nevertheless, a lot of these efforts are impeded by the diverse serotypes of the bacterium, which exhibit a high degree of variation and mutability. Consequently, vaccines targeting these antigens often provide protection only against homologous strain[8]. Despite the absence of clinically available vaccines for *P. aeruginosa*, the growing field of reverse vaccinology, which integrates structural biology, genetics, proteomics, and computational science, holds promise in providing novel preventive strategies[11].

In this investigation, we strive to create a multi-epitope vaccine to prevent *P. aeruginosa* infection via the integration of reverse vaccinology with immunoinformatics approaches (Fig. 1). 10 proteins were finally chosen for the vaccine, encompassing 10 epitopes for cytotoxic T lymphocyte (CTL), 10 epitopes for helper T lymphocyte (HTL), and 9 epitopes for linear B lymphocyte (LBL), all of which were identified through comprehensive screening and prediction techniques. This novel vaccine represents a promising alternative to treating infection with *P. aeruginosa*.

Materials and methods

Proteins screening and sequences acquisition

The target proteins were selected after conducting a literature review, with a focus on studies that demonstrated their protective effectiveness in mice[12–19]. UniProt database (https://www.uniprot.org/) consists of the amino acid sequences and extensive information about these proteins[20]. Subsequently, the PSORTb v3.0.2 server (https://www.psort.org/psortb/) was used together with the Gneg-PLoc 2.0 tool (http://www.csbio.sjtu.edu.cn/bioinf/Cell-PLoc-2/) to mutually validate the subcellular localization of the proteins, encompassing the cytoplasm, cytoplasmic membrane, periplasm, outer membrane, and extracellular space[21,22]. The DeepTMHMM server (https://dtu.biolib.com/DeepTMHMM) was employed to forecast transmembrane helices, and proteins with none or a single transmembrane helix were retained. Additionally, the SignalIP 6.0 server (https://services.healthtech.dtu.dk/services/SignalP-6.0/) was used to detect the signal sequence in target proteins. Proteins lacking a signal sequence or containing epitopes not located at the signal sequence position were selected for designing vaccine candidates[23]. Moreover, the Vaxijen v2.0 (https://www.ddg-pharmfac.net/vaxijen/VaxiJen/VaxiJen.html) and ProtParam (https://web.expasy.org/protparam/) servers were implemented to assess the antigenicity and the physicochemical properties of the proteins[24,25].

Eventually, we identified and included 10 proteins from *P. aeruginosa* (strain ATCC 15692), Type III secretion protein PcrV (UniProt ID: G3XD49), Beta-lactamase (UniProt ID: P24735), B-type flagellin (UniProt ID: P72151), Type IV major pilin protein PilA (UniProt ID: P04739), Fimbrial assembly protein PilQ (UniProt

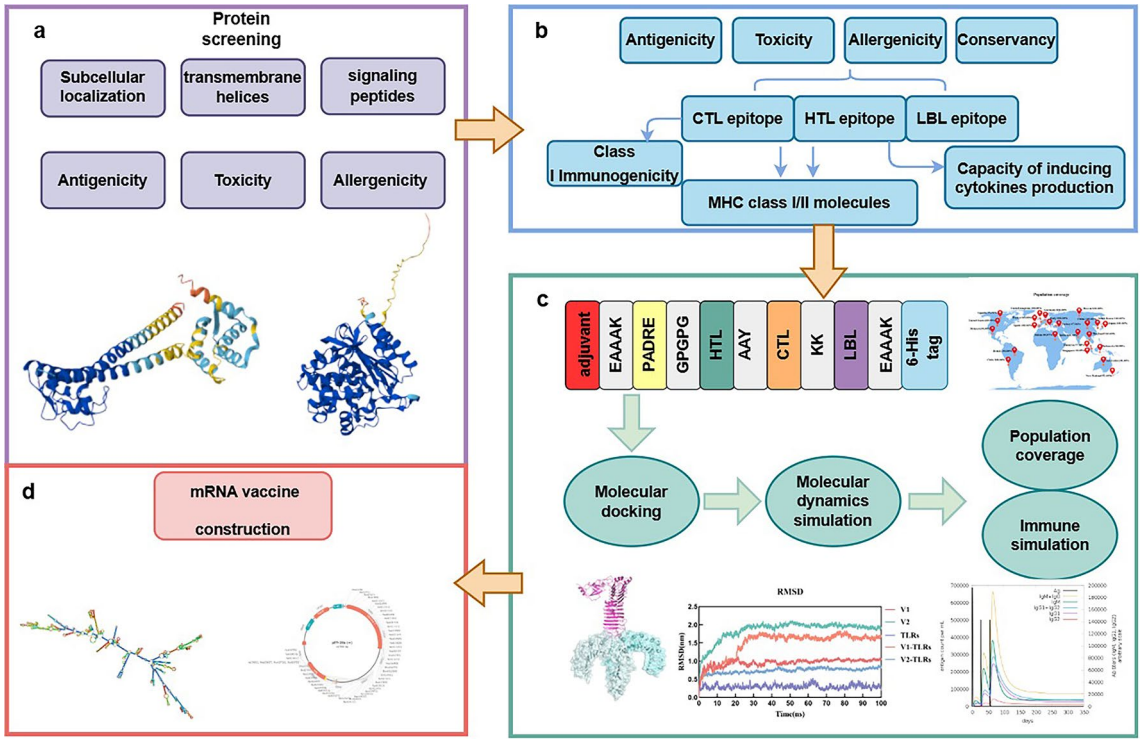

Fig. 1. The designing process of multi-epitope vaccine against *Pseudomonas aeruginosa*.

ID: P34750), Translocator protein PopB (UniProt ID: Q9I324), Protein Hcp1 (UniProt ID: Q9I747), Alginate biosynthesis protein (UniProt ID: Q51372), Exotoxin A (UniProt ID: P11439), Chitin-binding protein CbpD (UniProt ID: Q9I589).

Epitopes prediction and screening

T cell epitopes prediction and screening

CTLs provide a pivotal function in the human immune system through targeting and eliminating infected and cancerous cells. The use of NetMHCpan-4.1, as opposed to NetMHCpan-4.0, consistently improves the prediction accuracy of CTL epitopes for HLA-B and HLA-C molecules in terms of both epitopes and ligand benchmarks[26]. The NetMHCpan-4.1(https://services.healthtech.dtu.dk/services/NetMHCpan-4.1/) was utilized for predicting the binding MHC class I supertypes and their binding affinity, with the CTL epitope length being limited to 9mers and the threshold set at 0.5[27,28]. Identified strong binding epitopes were subsequently transmitted to the Vaxijen v2.0 server[29] (https://www.ddg-pharmfac.net/vaxijen/VaxiJen/VaxiJen.html), with epitopes exceeding the 0.4 thresholds further analyzed in the AllerTOP v2.0 (https://www.ddg-pharmfac.net/AllerTOP/) and ToxinPred 3 (https://webs.iiitd.edu.in/raghava/toxinpred3/) servers[30,31], respectively. Epitopes without toxicity and allergenicity were uploaded to Class I Immunogenicity within the IEDB database (http://tools.iedb.org/immunogenicity/) for the assessment of immunogenicity, where epitopes with values exceeding 0 were selected. Additionally, the TepiTool of the IEDB database was employed to forecast the binding of MHC class I molecules to epitopes. In this research, peptides having a predicted consensus percentile rank of ≤ 1% were deemed promising for future vaccine construction[32].

HTLs perform an essential part in human immune defense by activating and proliferating cytotoxic T lymphocytes, while also being capable of differentiating into cytotoxic CD4 + T cells that kill target cells directly. The MHC-II Binding of the IEDB database (https://www.iedb.org/) was employed to identify HTL epitopes, focusing on those with a percentile rank score of ≤ 1% for further examination[28,32]. Further scrutiny of epitopes satisfying the criteria of an antigenicity score greater than 0.4, as well as being non-toxic and non-allergenic, was conducted using TepiTool from the IEDB database. This analysis specifically focused on epitopes that bind to MHC-II molecules with percentiles below 2%. Furthermore, The interferon-γ and Interleukin-4 are secreted by CD4 + T cells, which are potent mediators of Th1 type immune response and Th2 type immune response, respectively[33–36]. The IFNepitope (https://webs.iiitd.edu.in/raghava/ifnepitope/predict.php) and IL-4pred (https://webs.iiitd.edu.in/raghava/il4pred/predict.php) tools were implemented to forecast the capability of the identified HTL epitopes to stimulate the production of interferon -γ or IL-4 respectively[35,36].

Furthermore, the crystal structures of MHC molecules were obtained from Protein Data Bank[37] (https://www.rcsb.org/) and their homology models were then created using SWISS-MODEL[38] (https://swissmodel.expasy.org/). The molecular docking between T cell epitopes and their MHC molecules was conducted using CABS-dock (https://biocomp.chem.uw.edu.pl/CABSdock) and visualized with PyMOL v2.5 software[39,40] (https://pymol.org).

B cell epitopes prediction and screening

As a pivotal component of the adaptive immune system, B Lymphocytes trigger and optimize a humoral immune response relying on the interaction between BCRs and B-cell epitopes. The ABCpred server (https://webs.iiitd.edu.in/raghava/abcpred/), utilizing a recurrent neural network was implemented to forecast linear B lymphocyte (LBL) epitopes[41,42]. For this investigation, the length of LBL epitopes was constrained to 16mer, with the threshold set at 0.51. Furthermore, by using a methodology and selecting criteria equivalent to the T cell epitopes screening, LBL epitopes were appropriately antigenic, with no toxicity or allergenicity.

Conservative analysis of epitope

Epitope Conservancy Analysis, a feature of the IEDB database (http://tools.iedb.org/conservancy/), is a tool for researching the variability or conservation of epitopes to promote advances in epitope-based vaccines and diagnostic procedures[43]. Further assessment was implemented into the Epitope Conservancy Analysis tool within IEDB to align with their respective target protein sequences from the UniProt database (https://www.uniprot.org/). Subsequently, epitopes possessing a conservation rate of more than 95% were chosen for the development of novel vaccines.

Vaccine structure construction

Epitopes with an antigenicity greater than 0.5, immunogenicity exceeding 0, and conservation of more than 95%, as well as being non-toxic and allergen-free, were used to construct the vaccine. GPGPG, AAY, and KK linkers were interposed among the HTL epitopes, CTL epitopes, and B-cell epitopes to enable the proper connection. The GPGPG linkers were used to allow the connected domains and facilitate antigen processing, while AAY linkers can provide proteasome cleavage sites and increase protein stability. The KK linkers are mainly related to the independent immune activity of the vaccine[44–47]. Human Beta-Defensin 3 (HBD3) is a naturally occurring cationic antimicrobial peptide generated from epithelial cells. PorB is a major outer membrane protein from *Neisseria meningitides* and is able to significantly increase co-stimulatory ligand expression and cytokine production in antigen presenting cells[48,49]. Both HBD3 and PorB can enhance vaccine efficacy by activating antigen-presenting cells through interactions with TLR1 and TLR2[50–52]. The HBD3 and the PorB sequence were widely chosen as adjuvant to promote the immune responses to the multi-epitope vaccine. The PADRE sequence has been recognized to elicit the HTL responses indispensable for generating antibodies specific to bacterial carbohydrates[53]. EAAAK, as a rigid linker, can optimize the function of the PADRE sequence by forming stable three-dimensional structures and be used to connect HBD3 and the PADRE sequence[54,55]. In addition, a 6×His tag positioned at the C-terminus of the vaccine acted as a protein purification marker.

Physicochemical properties of vaccine

The antigenicity of the candidate vaccines was evaluated with two servers: the VaxiJen 2.0 (https://www.ddg-pharmfac.net/vaxijen/VaxiJen/VaxiJen.html) and the ANTIGENpro (http://scratch.proteomics.ics.uci.edu/). To verify the vaccine's safety, we employed the AllerTOP v.2.0 (https://www.ddg-pharmfac.net/AllerTOP/) and the ToxinPred 2 (https://webs.iiitd.edu.in/raghava/toxinpred2/) servers to find out whether it was allergic or toxic. The physical and chemical properties of the proposed vaccine, including its molecule weight, amino acid count, and theoretical pI were determined with the ProtParam server[25] (https://web.expasy.org/protparam/). To detect whether the vaccine exhibits transmembrane helices and signal peptides, the DeepTMHMM (https://dtu.biolib.com/DeepTMHMM) and SignalP 6.0 (https://services.healthtech.dtu.dk/services/SignalP-6.0/) servers were applied. Additionally, the SOLpro server, a component of the Scratch server (http://scratch.proteomics.ics.uci.edu/), was implemented to estimate the vaccine's solubility potential when it was excessively expressed in *E. coli*.

Vaccine secondary and tertiary structures prediction, discontinuous B cell epitopes prediction

The PSIPRED 4.0 algorithm (http://bioinf.cs.ucl.ac.uk/psipred/), a highly esteemed tool for analyzing the secondary structural characteristics of the vaccine candidate, was employed in this investigation[56]. The vaccine's tertiary structure model was performed utilizing the Robetta server[57] (https://robetta.bakerlab.org/), followed by refinement in 3Drefine[58] (http://sysbio.rnet.missouri.edu/3Drefine/). To further validate the model, the refined version was examined through SAVESv6.0 (https://saves.mbi.ucla.edu/) to obtain the ERRAT score, which reveals error regions in protein crystal structures by studying pairwise atomic interactions; a higher score implies better model quality[59]. The PROCHECK tool was employed to generate the Ramachandran plot, with more than 90% of residues in favored regions supporting an acceptable structure. Further, the ProSA-web server (https://prosa.services.came.sbg.ac.at/prosa.php), another widely adopted tool, identified probable flaws in protein structures. The Z score represents overall model quality, whereas the energy plot displays local model quality via graphing a function of amino acid sequence position[60].

The discontinuous B cell epitopes are formed by folding far-apart residues in the protein sequence into spatial clusters, which are recognized antibodies and induce humoral immune response[61,62]. Then, the IEDB ElliPro tool (http://tools.iedb.org/ellipro/) was applied to predict the discontinuous B cell epitopes of the refined vaccines' structure[63,64].

Molecular docking

The binding modes and interactions between the molecules of the designed vaccine and Toll-like receptors were elucidated through molecular docking. TLR1 and TLR2 play a crucial role in microbial infection, regulation of signaling pathways, dendritic cell maturation, and T helper cell differentiation. Additionally, TLR2 is particularly known for its involvement in recognizing a wide range of microbial components, partly due to its synergistic interactions with other TLRs, such as TLR1 and TLR6[65]. Given their central role in immune responses, we selected TLR1 and TLR2 for molecular docking with the designed vaccine. By applying the ClusPro 2.0 server (https://cluspro.org/help.php), the molecule-specific docking models were created, allowing for the development of several docking models that were sorted according to their cluster scores[66]. The HADDOCK 2.4 server (https://rascar.science.uu.nl/haddock2.4/) was then implemented to improve the models with the lowest cluster scores to minimize the energy of the vaccine-TLR complexes and optimize the side-chain conformations of interfacial residues[67]. Furthermore, the PDBsum server (https://www.ebi.ac.uk/thornton-srv/databases/pdbsum/) was utilized to identify which amino acid residues participated in the interaction between the vaccine and TLRs[68].

Analysis of molecular dynamics simulation

Molecular dynamics simulation

We employed GROMACS v2022.3 software (GROningen MAchine for Chemical Simulations v2022.3, https://www.gromacs.org) to perform molecular dynamics simulations and analyze their trajectories to deeply explore the optimal balance of the post-docking vaccine-TLRs complex[69]. The Amber99SB-ILDN force field, recognized as one of the positions suitable for simulating protein complexes, was employed to elucidate the initial conformation of the vaccine-TLRs complex, enabling the generation of coordinate files and topology[70]. Subsequently, the system was solvated by introducing TIP3P water molecules for proper hydration, then completing electrical neutralization with Na + or Cl − ions. Energy minimization was carried out iteratively until convergence was attained. For maintaining the isothermal and isobaric circumstances, NVT (isothermal isovolumetric) and NPT (isothermal isobaric) simulations were performed for 400ps and 1 ns, until the temperature and the pressure of the system were 310 K and 1 atm. Temperature and pressure equilibrium were achieved by utilizing an improved Berendsen thermostat and a Parinello-Rahman barostat. Following the simulations, several structural metrics involving Root Mean Square Deviation, Root Mean Square Fluctuation, Radius of Gyration, and hydrogen bonding were assessed across a 100 ns molecular dynamics trajectory under isothermal and isobaric circumstances. Hydrogen bonds was confined using the LINCS algorithm, whereas distant electrostatic interactions were approximated via the Particle-Mesh Ewald theory.

MM-PBSA calculation

We selected the ultimate ten nanoseconds from the molecular dynamics trajectories for analyzing and estimating the binding free energy of the vaccine-TLR1 and vaccine-TLR2 with the gmx_MMPBSA v1.61 tool, depending on the Molecular Mechanics/Poisson-Boltzmann surface area technique[71].

Immune simulation

Leveraging a rapid Position Specific Scoring Matrix (PSSM)-based method, the C-ImmSim website (https://kraken.iac.rm.cnr.it/C-IMMSIM/index.php) was deployed to simulate and evaluate the immunological reaction expected in humans[72,73]. The vaccination protocol involved a total of 1050 simulation steps (350 days), including three injections given at time step 1, 86, and 164, each separated by four weeks[74], with 1000 vaccine units administered each time. Other parameters remained default values.

Population coverage prediction

MHC molecules, recognized for their polymorphism, reveal how distinct geographical regions and ethnic populations display distinct distributions of HLA alleles. To evaluate the proposed vaccine's worldwide population coverage, the Population Coverage tool of the IEDB (http://tools.iedb.org/population/) was implemented, revealing its potential for widespread implementation[75].

Disulfide engineering of the vaccine

Disulfide bonds play an important role in maintaining the stability of protein conformation. The Disulfide by Design 2 server (http://cptweb.cpt.wayne.edu/DbD2/) was utilized to conduct the disulfide engineering of the refined vaccine[76]. The residue pairs that were not located in epitopes and exhibited an energy value < 2.2 kcal/mol and a $\chi 3$ angle between − 87° and + 97°± 30 were selected to form disulfide bonds. The PyMOL v2.5 software was used to visualize the selected residue pairs.

mRNA vaccine

Codon optimizing and computational cloning

The EMBOSS server (https://emboss.sourceforge.net/servers/), an application for DNA and protein sequence analysis[77], was used to realize the transformation of vaccine sequence and DNA sequence. The JCat server (http://www.prodoric.de/JCat) provides a platform to optimize the vaccine's codon usage by excluding cleavage sites for specific restriction enzymes and avoiding Rho-independent transcription terminators in the codon-optimized DNA sequence[78]. Significantly, we used the Codon Adaptation Index Calculator and the GC Content Calculator of the BiologicsCorp website (https://www.biologicscorp.com/tools/GCContent/) to determine the Codon Adaptation Index (CAI) and the GC content percentage, both of which functioned as indices to determine the degree of mRNA sequence expression. The CAI value reflects the expression level of genes[79], while the GC content value indicates effective transcription and translation. The optimized codon sequence was modified to contain XhoI and BamHI restriction endonuclease sites at the C-terminus and N-terminus. The expression vector chosen was *E. coli* (Strain K12). Additionally, pET-28a (+) is the most commonly used expression plasmid vector because of its high yield and product yield in *E. coli* expression systems[80]. Subsequently, the generated sequence was integrated into the pET-28a (+) vector through the GenSmart website (https://www.genscript.com/gene-and-plasmid-construct-design.html).

Designing mRNA vaccine

The mRNA vaccine was engineered using a combination of several vital components. The Tissue Plasminogen Activator (tPA) and the MHC I-targeting domain (MITD) sequences were attached to each end of the vaccine sequence. The MITD sequence makes it easier for MHC molecules to be presented, whereas the tPA sequence improves the sequence's transfer across the cytomembrane. A TAA stop codon and a Kozak motif were appended at the 5' and 3' termini of the DNA sequence respectively. Furthermore, Homology arms and spacers were strategically placed flanking the DNA sequence. Subsequently, the complete DNA sequences were transcribed into mRNA sequences.

The RNAfold website (http://rna.tbi.univie.ac.at/) was implemented to figure out the secondary structure of vaccine mRNA using John McCaskill's algorithm and partition function (PF) algorithm[81]. The output included the minimal free energy (MFE), detailed secondary structure, and centroid secondary structure. A lower MFE value signifies a more stable folding structure for the mRNA vaccine.

Results

Sequence acquisition and epitope screening

Following an exhaustive literature retrieval, the proteins were screened based on a variety of criteria. Subsequently, 10 proteins were identified as antigenic, without allergy, toxicity, or homology with human proteins, stable, and possessing an optimal molecular weight, culminating in their selection for the vaccine. (Table 1)

Upon conducting a comprehensive prediction and screening process, candidate epitopes should exhibit highly conserved, antigenic, free of toxicity and allergies. Additionally, the capability to trigger the production of interferon-γ and interleukin-4 of HTL epitopes is taken into account. Ultimately, this study identified 10 CTL epitopes (Table 2, Supplementary Table S1), 10 HTL epitopes (Table 3), and 9 LBL epitopes (Table 4) for vaccine development. The molecular docking between CTL epitopes and MHC-I molecules, as well as between HTL epitopes and MHC-II molecules were shown in (Supplementary Fig. S1, Supplementary Fig.S2).

Vaccine construction and property assessment

Two vaccines were finally designed, labeled V1 and V2 based on different adjuvants (HBD3 and PorB sequences). Figure 2 illustrates the primary and secondary structures of these two vaccines. To ascertain the security and antigenicity of the multi-epitope vaccines, the vaccine sequences were subjected to ToxinPred2, AllerTOP v.2.0, and VaxiJen2.0, confirming their lack of toxicity and allergenicity, yielding antigenicity values of 1.1137 for V1 and 1.0805 for V2. Additionally, the physicochemical properties of V1 and V2 were evaluated using the ProtParam server. V1 had 556 amino acids, a molecule weight of 58.851 kDa, and a theoretical pI of 9.20. its instability

Protein	Uniprot ID	Subcellular localization		Antigenicity	Instability index	Aliphatic index	Grand average of hydropathicity (GRAVY)	Transmembrane helix cont	Signal
		PSORTb v3.0.2	Gneg-PLoc 2.0						
Type III secretion protein PcrV	G3XD49	Extracellular	Extracell	0.4372	41.07(unstable)	101.94	−0.257	0	0
Beta-lactamase	P24735	Periplasmic	Periplasm	0.5231	35.95(stable)	85.42	−0.290	0	1
B-type flagellin	P72151	Extracellular	Extracell	0.8011	15.81(stable)	89.34	−0.077	0	0
Type IV major pilin protein PilA	P04739	Extracellular	Cell inner membrane	0.6418	31.38(stable)	92.42	0.130	1	1
Fimbrial assembly protein PilQ	P34750	OuterMembrane	Cell outer membrane	0.6591	35.57(stable)	95.88	−0.257	0	1
Translocator protein PopB	Q9I324	Extracellular	Cell inner membrane	0.5577	36.46(stable)	103.26	0.164	0	0
Protein Hcp1	Q9I747	Extracellular	Extracell	1.2709	38.34(stable)	72.78	−0.415	0	0
Alginate biosynthesis protein AlgX	Q51372	Periplasmic	Periplasm	0.4393	44.89(unstable)	74.01	−0.430	0	1
Exotoxin A	P11439	Extracellular	Cell inner membrane	0.4725	38.80(stable)	88.78	−0.262	0	1
Chitin-binding protein CbpD	Q9I589	Extracellular	Extracell	0.6579	35.14(stable)	70.85	−0.352	0	1

Table 1. Selected *P. aeruginosa* proteins.

Protein	Uniport ID	Start position	CTL Epitope	Antigenicity	Toxicity	Immunogenicity	Allergenicity	Conservative property ≤ 100%
Type III secretion protein PcrV	G3XD49	108	RLDEDVIGV	1.3936	–	0.30053	–	99.45% (2181/2193)
Beta-lactamase	P24735	299	EAYDWPISL	1.2674	–	0.24204	–	95.08% (1238/1302)
B-type flagellin	P72151	224	KMDGAIPNL	1.1049	–	0.19154	–	99.84% (1268/1270)
Type IV major pilin protein PilA	P04739	100	GAGDITFTF	1.7755	–	0.32094	–	95.38% (62/65)
Fimbrial assembly protein PilQ	P34750	528	ATSGIGIGF	1.7655	–	0.27402	–	100.00% (566/566)
Translocator protein PopB	Q9I324	47	SASGTGVAL	2.0482	–	0.1078	–	97.66% (1170/1198)
Protein Hcp1	Q9I747	26	DVLAWSWGM	1.7210	–	0.30248	–	99.05% (1144/1155)
Alginate biosynthesis protein AlgX	Q51372	320	LIWEFATHY	1.0561	–	0.37514	–	100.00% (1263/1263)
Exotoxin A	P11439	359	EQARLALTL	0.7535	–	0.10413	–	97.98% (3347/3416)
Chitin-binding protein CbpD	Q9I589	164	SVKLENGTY	1.1065	–	0.06153	–	99.04% (2987/3016)

Table 2. The cytotoxic T cell (CTL) epitopes.

index, aliphatic index, and GRAVY are 16.91, 65.81, and − 0.442, respectively. V1's estimated half-life is 30 h in mammalian reticulocytes, over 20 h in yeast, and 10 h in *E. coli*. On the other hand, V2 exhibited 586 amino acids, a molecule weight of 61.271 kDa, and a theoretical pI of 7.88. The values of instability, aliphatic index, and GRAVY were 13.42, 70.78, and − 0.330. The estimated half-life of V2 is 20 h in mammalian reticulocytes, over 30 min in yeast, and more than 10 h in *E. coli*. Solubility analysis conducted using the SOLpro server indicated both vaccines were soluble, with solubility values of 0.945806 for V1 and 0.874233 for V2. Finally, assessments by the DeepTMHMM server and SignalP 6.0 server revealed that neither vaccine possesses transmembrane helices nor signal peptides (Table 5).

Secondary and tertiary structure construction, discontinuous B cell epitopes prediction

Results from the PSIPRED 4.0 analysis revealed the secondary structure compositions of the two vaccines (Fig. 2B, D), V1 was comprised of 53.42% coils, 26.80% helices, and 3.42% strands, whereas V2 consisted of 55.63% coils, 21.67% helices, and 3.58% strands. The vaccine models were automatically generated by the Robetta server and refined using 3Drefine to optimize their structures. The refined models of V1 and V2 achieved MolProbity scores of 1.672 and 1.129, respectively. Subsequently, the SAVESv6.0 server and ProSA-web validated these models, demonstrating their reasonable structures. The ERRAT score and Z-score for V1 were 94.189 and − 5.84, while V2 received an ERRAT score of 89.844 and a Z-score of −3.36. PROCHECK analysis showed that the Ramachandran plots of both vaccines displayed significant amounts of residues in the most favored regions, with V1 having 96.4% in the most favored regions, 3.6% in additional allowed regions, and none in disallowed regions. In contrast, the V2 vaccine displayed 94.2% residues in the most favored regions, 5.4% in additional allowed regions, and 0.4% residues in generously allowed regions. In comparison with the original models (V1 exhibited 86.0% residues in most favored regions, V2 exhibited 83.9% residues in most favored regions), these findings indicate that both vaccines exhibit good structural quality, with more than 90% of residues in the most desired locations (Fig. 3, Supplementary Fig.S3). Additionally, results from the IEDB ElliPro tool showed that there were 25 discontinuous B cell epitopes of the refined V1 structure and 9 discontinuous B cell epitopes of the refined V2 structure (Supplementary Table S2, Supplementary Fig.S4).

Protein	Uniport ID	Start position	HTL Epitope	HLA-II alleles	Antigenicity	Toxicity	Allergenicity	IFN-γinduction	IL-4 induction	Conservative property ≤ 100%
Type III secretion protein PcrV	G3XD49	174	PTLYGYAVGDPRWKD	HLA-DRB5*01:01	0.7122	–	–	+	+	98.13% (2152/2193)
Beta-lactamase	P24735	160	DYYRQWQPTYAPGSQ	HLA-DQA1*04:01/DQB1*04:02	0.6359	–	–	+	+	95.47% (1243/1302)
B-type flagellin	P72151	306	NVKFGAQTGTATAGQ	HLA-DRB1*01:01	1.6557	–	–	–	+	98.82% (1255/1270)
Type IV major pilin protein PilA	P04739	30	YQNYVARSEGASALA	HLA-DQA1*04:01/DQB1*04:02 HLA-DRB1*08:02	0.5035	–	–	+	–	100.00% (65/65)
Fimbrial assembly protein PilQ	P34750	163	IRNIDFQRGEKGEGN	HLA-DRB1*01:01 HLA-DRB4*01:01	1.8209	–	–	+	+	100.00% (566/566)
Translocator protein PopB	Q9I324	306	DLTLDVANGAAQATH	HLA-DQA1*05:01/DQB1*03:01	1.0188	–	–	–	–	95.08% (1139/1198)
Protein Hcp1	Q9I747	123	ENVTLNFAQVQVDYQ	HLA-DQA1*03:01/DQB1*03:02	0.8291	–	–	+	+	99.05% (1144/1155)
Alginate biosynthesis protein AlgX	Q51372	310	EEFHKNPPKILIWEF	HLA-DRB3*02:02	1.0574	–	–	+	+	99.76% (1260/1263)
Exotoxin A	P11439	259	KHDLDIKPTVISHRL	HLA-DRB1*08:02	1.5252	–	–	+	+	99.68% (3405/3416)
Chitin-binding protein CbpD	Q9I589	234	TVTLRLFDAQGRDAQ	HLA-DPA1*02:01/DPB1*05:01 HLA-DRB1*13:02 HLA-DRB1*15:01 HLA-DRB5*01:01	1.4230	–	–	+	–	99.87% (3012/3016)

Table 3. The helper T cell (HTL) epitopes.

Protein	Uniport ID	Start position	LBL Epitope	Antigenicity	Toxicity	Allergenicity	Conservative property ≤ 100%
Type III secretion protein PcrV	G3XD49	88	PGAQWDLREFLVSAYF	1.0152	–	–	99.36% (2179/2193)
Beta-lactamase	P24735	253	TSAADLLRFVDANLHP	0.5091	–	–	97.93% (1275/1302)
B-type flagellin	P72151	300	TSATGENVKFGAQTGT	1.5601	–	–	99.53% (1264/1270)
Fimbrial assembly protein PilQ	P34750	404	GQEGKEGGRGSITVDD	2.2767	–	–	99.47% (563/566)
Translocator protein PopB	Q9I324	182	VGAIMVATGVGAAAGA	0.5339	–	–	98.75% (1183/1198)
Protein Hcp1	Q9I747	114	GSGGEDRLTENVTLNF	2.1186	–	–	99.05% (1144/1155)
Alginate biosynthesis protein AlgX	Q51372	414	SKAVDTGGRYVFQLRN	0.9500	–	–	99.76% (1260/1263)
Exotoxin A	P11439	564	LDAITGPEEEGGRLET	1.1612	–	–	99.68% (3405/3416)
Chitin-binding protein CbpD	Q9I589	125	ASAPHATRYFDFYITK	0.7185	–	–	99.97% (3015/3016)

Table 4. The linear B cell (LBL) epitopes.

Vaccine-TLR complexes molecular docking

The ClusPro 2.0 server and HADDOCK 2.4 server were utilized to generate molecular docking models of vaccine-TLR complexes. The most favorable model was selected for further analysis based on superior binding characteristics. The HADDOCK scores of the V1-TLRs model and V2-TLRs model are -265.5 ± 3.0 and -343.2 ± 5.6, demonstrating a strong binding affinity. Detailed interactions between the vaccines and TLRs were elucidated using results obtained from the PDBsum server (Fig. 4). The V1 vaccine and TLR1 formed 4 H-bonds and 1 salt bridge, while 10 H-bonds and 1 salt bridge were identified with TLR2. The V2 vaccine developed 8 H-bonds with TLR1, but 9 H-bonds and 1 salt bridge with TLR2. Notably, the V2-TLRs complex exhibited a better docking impact due to the higher amount of hydrogen bonds established (Supplementary Table S3).

Analysis of molecular dynamics simulation

We used Gromacs v2023.3 to analyze the molecular dynamics trajectory of the models of vaccine-TLR complexes, V1, V2, TLR1, and TLR2 in this investigation, which illustrated structure changes during a 100 ns period (Fig. 5, Supplementary Fig.S5). The Root Mean Square Deviation (RMSD) was employed as a quantifiable statistic to demonstrate conformational variances at the atomic level between the simulated structures and their original forms. In the V1-TLRs complex, the curve of RMSD values exhibited an initial erratic growth during the first 10 ns, reaching its first equilibrium at 6 ns, followed by an ongoing increasing trend until achieving another

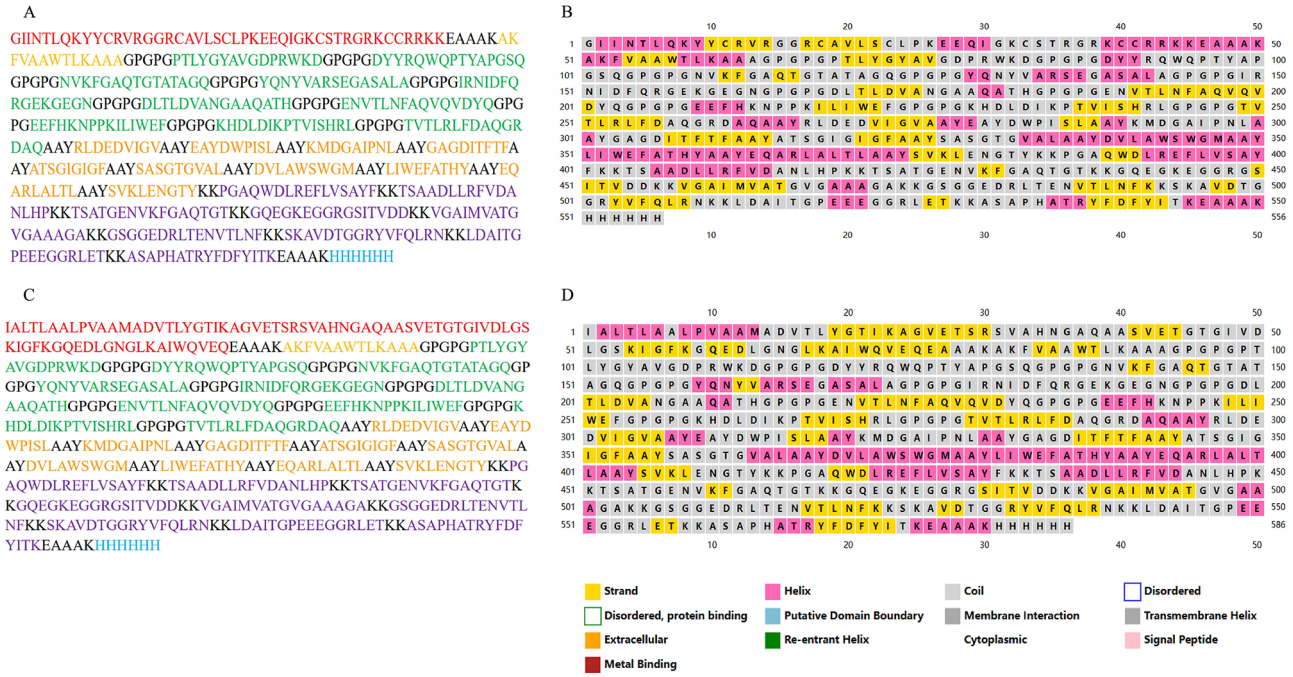

Fig. 2. The amino acid sequences and secondary structures of vaccines (Red: adjuvant; Black: linker; Yellow: PADRE; Green: HTL epitope; Orange: CTL epitope; Purple: LBL epitope; Blue: 6×His tag). (**A**, **B**) The amino acid sequences and secondary structures of V1;(**C**, **D**) The amino acid sequences and secondary structures of V2.

equilibrium point at 33 ns. Subsequently, after 33 ns, the RMSD stabilizes with slight fluctuations, signifying the attainment of stability in the V1-TLRs complex. On the other hand, for the V2-TLRs complex, the RMSD curve stabilized within the first 10 ns, reaching a peak value of 0.7 nm around 1–2 ns, and maintained this steadiness for the remainder of the simulation The average RMAD values for V1-TLRs and V2-TLRs complexes were 1.480 ± 0.3434 nm and 0.7412 ± 0.0705 nm, respectively. (Fig. 5A). The V2-TLRs complex demonstrates greater stability compared to the V1-TLRs complex.

The radius of gyration (Rg), an indicator of the root-mean-square distance between all atoms and their centroid in a molecule, was utilized to evaluate the tightness of the complex. The Rg curve of the V1-TLRs complex demonstrated an initial decrease within the first 30 ns, followed by reaching a relatively stable state thereafter, consistently higher than that of the V2-TLRs complex. In contrast, the Rg curve of the V2-TLRs complex maintained a stable and lower value throughout the MD simulation. The mean Rg value for the V1-TLRs complex was 4.696 ± 0.1772 nm, whereas, for the V2-TLRs complex, it was 4.352 ± 0.03887 nm. These findings suggest that the V2 and V2-TLRs complex exhibits a tighter structure (Fig. 5B, C).

The number of hydrogen bonds, measured as the force of interaction between molecules, was utilized to determine the binding affinity of vaccine-TLR complexes. For the intermolecular of vaccine and TLRs, both V1-TLRs complex and V2-TLRs complex exhibited a gradual rise in the number of H-bonds, beginning with 14 in the initial structure and culminating at 30 for the V1-TLRs complex, with an average value of 16.54. In comparison, the count of the H-bond in the V2-TLRs complex ranged from 17 in the original structure to a maximum of 25, with an average value of 13.92 (Fig. 5E). The number of H-bond of V1 was slightly higher than V2 (Fig. 5D). Additionally, the average H-bond of the whole V1-TLRs complexes and the whole V2-TLRs complexes were 1144 and 1133, respectively. (Fig. 5F). Under these conditions, the V1 vaccine shows a higher binding affinity to TLRs.

The Root Mean Square Fluctuation (RMSF), serves as an indicator of the flexibility of amino acid residues within a protein molecule, measuring the deviations of each atom's position from its average position in the molecule. Higher RMSF values indicate increased flexibility in the vaccine-TLRs complex. While both the curves of RMSF showed a decreasing trend in the vaccine and TLR1, TLR2 exhibited an increasing trend. In the V1-TLRs complex, the TLR2 chain displayed more pronounced changes in RMSF values compared to the other two chains, particularly evident in residues after 370, suggesting that the residues display higher variations throughout the MD simulation. The fluctuation of the V1 vaccine ranged from 0.2672 to 1.038, with a mean value of 0.5309 ± 0.1584 nm. Similarly, in the V2-TLRs complex, the RMSF values of TLR2 varied significantly in residues after 300, peaking at 0.5269 in residue 409. Furthermore, the V2 vaccine had a mean RMSF value of 0.2099 ± 0.05666 nm, with the maximal value of 0.4576 observed in residue 306 (Supplementary Fig.S5 A-B). Overall, the V1 vaccine exhibits higher flexibility compared to the V2 vaccine.

The free binding energies of the vaccine-TLRs complexes were revealed utilizing gmx_MMPBSA v1.61. The total binding free energies were determined to be −135.84 kcal/mol for V1-TLRs complex and − 105.00 kcal/mol for V2-TLRs complex at a temperature of 310.00 K, indicating that both complexes exhibit stable conformations,

Vaccine	Vaxijen v2.0	ANTIGEN pro	Toxicity	Allergenicity	Amino acid cont	Molecular weight	pI	The estimated half-life	Instability index	Aliphatic index	Grand average of hydropathicity (GRAVY)	Signal	Number of transmembrane helix	SOLpro
V1	1.1137	0.922072	Non-Toxin	NON-ALLERGEN	556	58851.18	9.20	30 h (mammalian reticulocytes) > 20 h (yeas) > 10 h (Escherichia coli)	16.91 (stable)	65.81	−0.442	0	0	0.945806
V2	1.0805	0.929835	Non-Toxin	NON-ALLERGEN	586	61271.61	7.88	20 h (mammalian reticulocytes) 30 min (yeas) > 10 h (Escherichia coli)	13.42 (stable)	70.78	−0.330	1	0	0.874233

Table 5. The prediction of the designed vaccine properties.

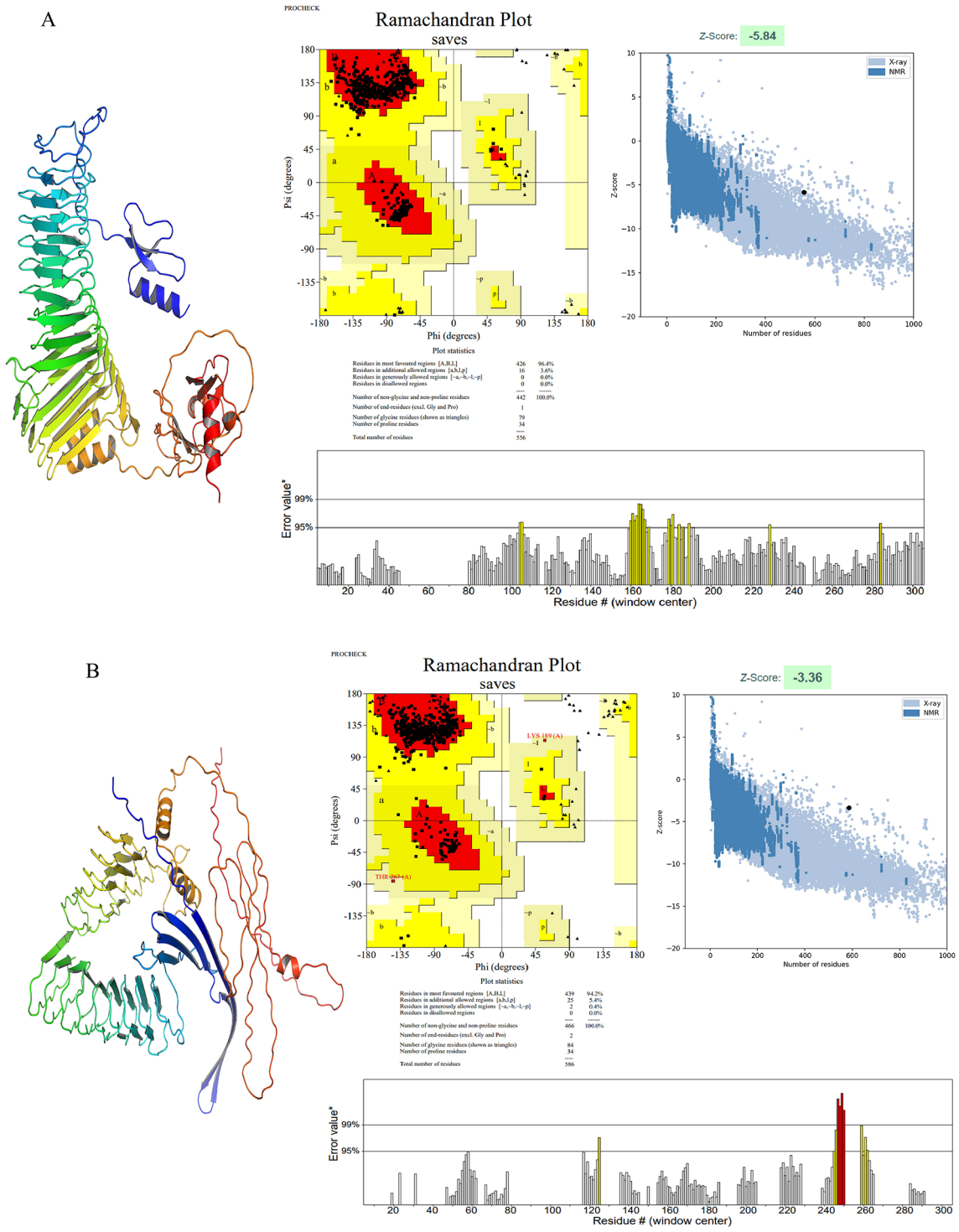

Fig. 3. Tertiary structure and quality analysis of vaccines. (**A**) Tertiary structure of V1 and its ERRAT scores, Ramachandran charts, Z-score, and energy charts; (**B**) Tertiary structure of V2 and its ERRAT scores, Ramachandran charts, Z-score, and energy charts.

with the V1-TLRs complex demonstrating relatively greater stability. Table 6 offers a detailed analysis of various interactions, such as van der Waals, electrostatic, polar solubility, solvent-accessible surface area, and binding energy.

Immune simulation

Employing immunological simulation with the C-ImmSim server, the efficacy of the developed vaccines in inducing an immune response and the dynamics of antibody-mediated and cell-mediated immunity after

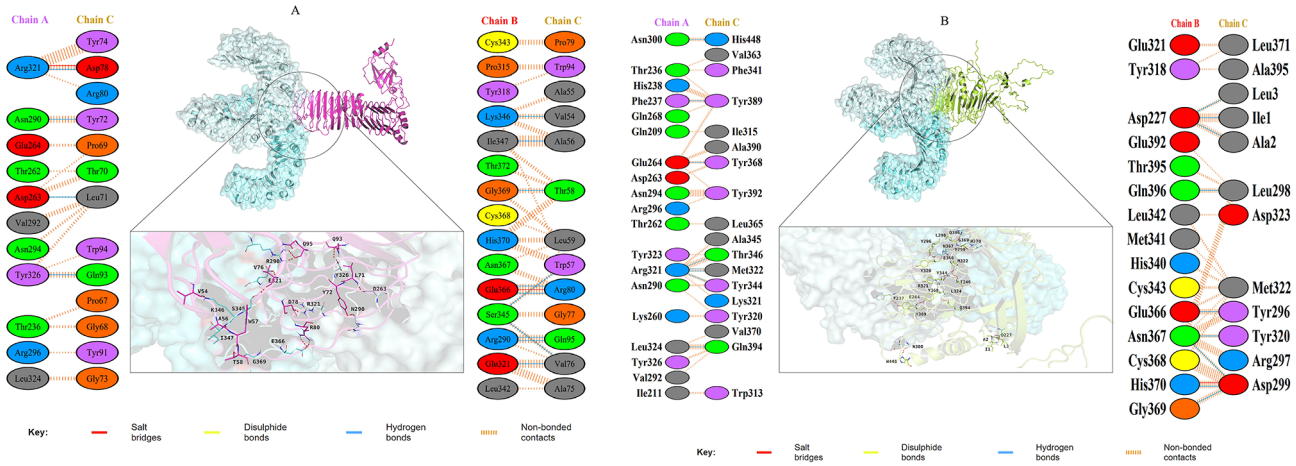

Fig. 4. Visualization and analysis of vaccine-TLR complexes. (**A**) V1-TLRs complex; (**B**) V1-TLRs complex.

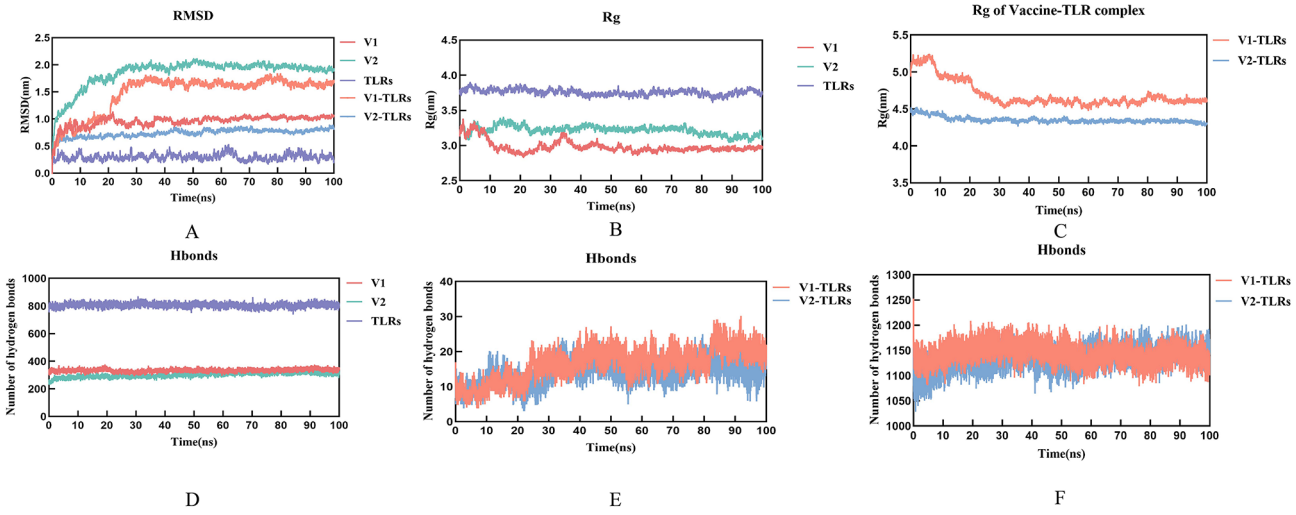

Fig. 5. Molecular dynamics analysis of vaccine-TLR complexes. (**A**) RMSD of V1, V2, TLRs, V1-TLRs complexes, and V2-TLRs complexes; (**B**) Rg of V1, V2, and TLRs; (**C**) Rg of V1-TLRs complexes and V2-TLRs complexes; (**D**) Hydrogen bonds of V1, V2, and TLRs; (**E**) Intermolecular Hydrogen bonds of V1-TLRs and V2-TLRs; (**F**) Total Hydrogen bonds of V1-TLRs complexes and V2-TLRs complexes.

Complex	ΔVDWAALS Average (SD)	ΔEEL Average (SD)	ΔEPB Average (SD)	ΔENPOLAR Average (SD)	ΔGGAS Average (SD)	ΔGSOLV Average (SD)	ΔTOTAL Average (SD)
Vaccine1-TLRs	−153.00(8.36)	−1182.79(68.17)	1217.39(67.18)	−19.44(0.71)	−1335.79(69.70)	1199.95(66.94)	−135.84(10.54)
Vaccine2-TLRs	−170.27(9.68)	−401.98(52.48)	486.64(47.44)	−19.38(0.83)	−572.25(49.61)	467.25(47.41)	−105.00(12.92)

Table 6. The results from MMPBSA for the vaccine-TLRs complex (van der Waals interaction (ΔVDWAALS), electrostatic interaction (ΔEEL), polarization energy (ΔEPB), non-polar solvation energy (ΔENPOLAR), gas-phase energy (ΔGGAS), solvation energy (ΔGSOLV)).

vaccination were examined. In this investigation, the vaccination regimen lasted 350 days and tended to have sustained protective effects (Fig. 6). After the first dose was administered, the curves of antibodies, B cells, plasma cells, and TH cells increased slightly for both V1 and V2 vaccines, with more pronounced amplification after the second and third doses (Fig. 6A-C, E-G, Supplementary Fig.S6, S7 F). After a third injection at around 50 days, the IgM + IgG titers of V1 and V2 reached a peak of around 180,000 (Fig. 6A, B). Moreover, both vaccines induced notable cytokines production, including IL-2, IL-10, IL-18, IFN-γ, and TGF-β, with IL-2 showing a clear upward trend and IFN-γ possessing a high level of greater than 400,000 ng/ml (Fig. 6D, H). With the third vaccination, the active B cell population, TH cell population, and TC cell population of V1 peaked at about 700

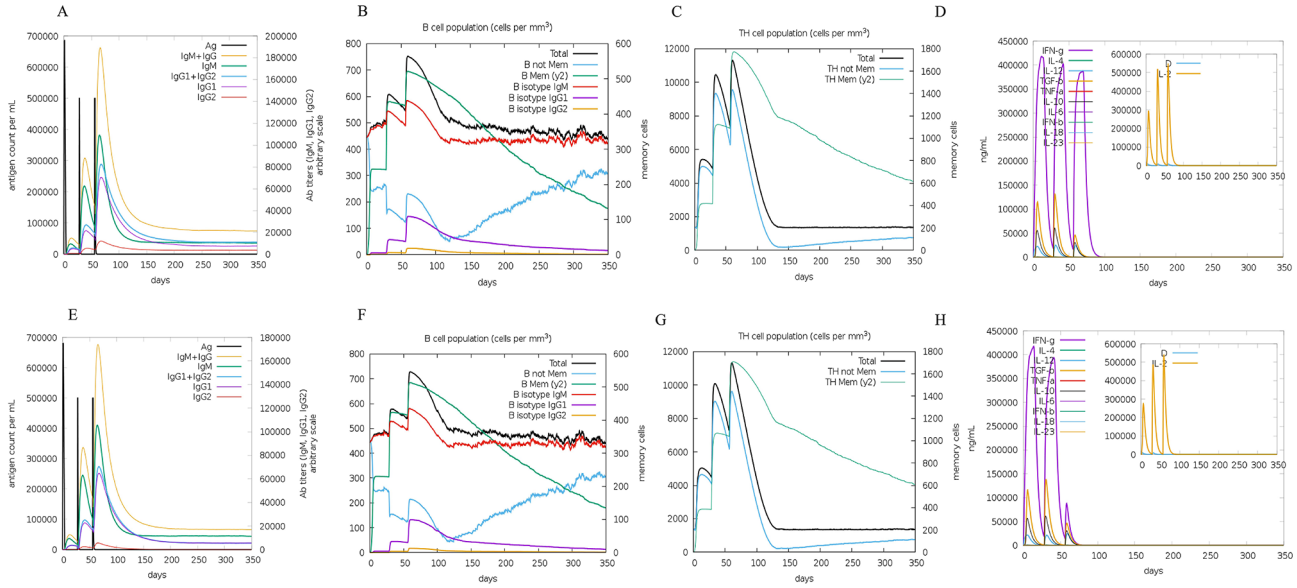

Fig. 6. Immune simulation results. (**A**, **E**) Antibody levels of V1 and V2;(**B**, **F**) B cell levels of V1 and V2;(**C**, **G**) TH cell levels of V1 and V2;(D, H) Cytokine levels of V1 and V2.

cells per mm^3, 8000 cells per mm^3, and 700 cell per mm^3, respectively. Similarly, the active B cell population, TH cell population, and TC cell population of V2 reached a crest value of 700 cells per mm^3, 7000 cells per mm^3, and 800 cell per mm^3, respectively (Supplementary Fig.S6, S7 A, B, D). The high amount of B lymphocyte and T lymphocytes indicated that the vaccines triggered sufficient humoral and cell immune responses. Both B memory cells and TH memory cells exhibited growth after each injection, but V1 induced a higher count of TH and TC memory cells compared to V2. The trajectory of B memory cells, TH memory cells, and TC memory cells continued until the conclusion of the immune simulation, suggesting a more enduring protective effect of the vaccines (Fig. 6B, C, F, G, Supplementary Fig.S6, S7 C). Additionally, the vaccines recruited Dendritic cells, Epithelial cells, Macrophage cells, and Natural Killer cells to enhance the immune response (Supplementary Fig. S6, S7 G-J). The analysis demonstrates that both V1 and V2 may elicit an effective immunological response in the human body.

Population coverage

The population coverage is estimated as an indicator of the number of individuals worldwide who would benefit from the effectiveness of vaccination across various regions. Data from the IEDB Population Coverage tool revealed that the multi-epitope vaccines exhibited a worldwide population coverage rate of 99.30%, with the majority of regions reaching 100.00%, highlighting the wide protective impact of the designed vaccines (Fig. 7).

Disulfide engineering of the vaccine

The analysis of Disulfide by Design 2 server suggested that the refined structure of V1 had 39 residue pairs with the potential to form disulfide bonds, whereas the refined structure of V2 exhibited 9 residue pairs with the potential to form disulfide bonds (Supplementary Data Sheet 1). Eventually, only 2 residue pairs located in adjuvant and satisfied the criteria of the energy value < 2.2 kcal/mol and the $\chi 3$ angle between −87° and +97°± 30 (GLY31- CYS40 of V1 and GLY56-GLU74 of V2) (Supplementary Fig.S8).

mRNA vaccine

The final DNA construct of vaccines, containing the tPA sequence, MITD sequence, Kozak sequence, TAA, 5'UTR, and 3'UTR, with a length of 2484 bp for V1 and 2574 bp for V2, respectively (Fig. 8A). After optimizing the mRNA vaccine sequences, we used the Codon Adaptation Index Calculator and the GC Content Calculator of the BiologicsCorp server to determine that V1 had a CAI value of 0.79 and a GC content of 69% for V1, while V2 exhibited a CAI value of 0.80 and a GC content of 69%, both of which were aligning well with the desired parameters. Finally, results from the GenSmart™ Design were illustrated in Fig. 8 (C, E), which demonstrated that both V1 and V2 were appropriately integrated into the pET-28a (+) vectors.

Results from the RNAfold website indicated that the optimal secondary structure of the V1 mRNA possessed a minimal free energy of −1174.40 kcal/mol, with −961.50 kcal/mol for its centroid secondary structure. In contrast, the optimal secondary structure of the V2 mRNA exhibited a minimal free energy of −1226.20 kcal/mol, with −927.12 kcal/mol for its centroid secondary structure (Fig. 8B, D). These findings suggest that the secondary structures of the mRNA vaccine are highly stable, allowing for practical development.

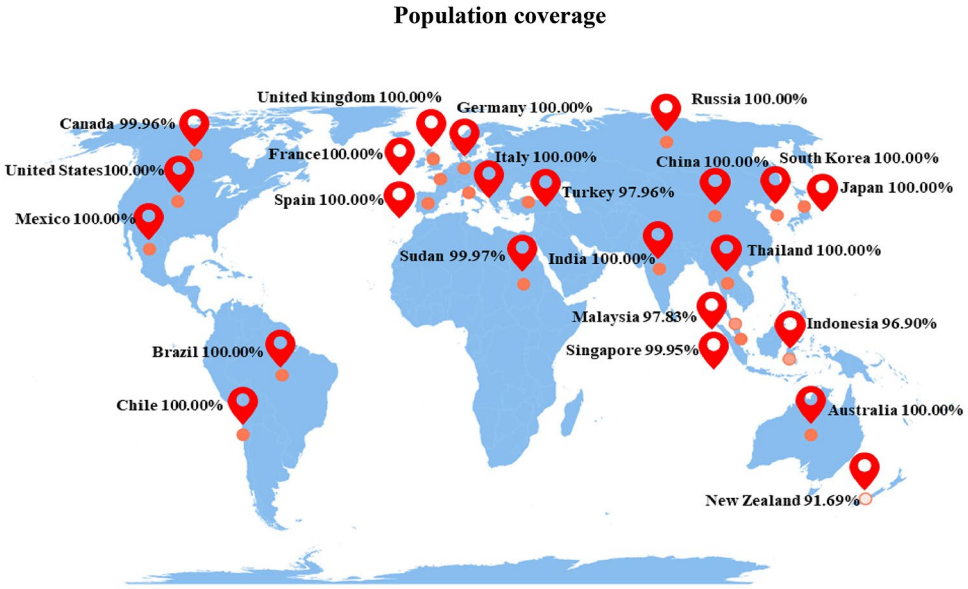

Fig. 7. Population coverage rate of V1 and V2.

Discussion

The opportunistic bacteria *Pseudomonas aeruginosa* is frequently linked to CF patients or complications following surgery, trauma, and thermal burns[82]. Categorized as an MDR pathogen, *P. aeruginosa*is resistant to almost all available antimicrobial drugs, posing a substantial challenge[83–85]. Designated by the WHO as one of the top bacteria necessitating new antibiotic development, carbapenem-resistant *P. aeruginosa* (CR-PA) presents an emerging threat[86,87]. Although vaccines have been developed to combat *P. aeruginosa* by effectively stimulating humoral and cellular immune responses through antigen recognition by antigen-presenting cells, these vaccines have not been successful in passing clinical trials for practical application[8]. Hence, a breakthrough of novel immunoprophylaxis as a substitute treatment for *P. aeruginosa* infections is of paramount importance. The advancement of reverse vaccinology has rendered it possible to create a cell-free mRNA vaccine for *P. aeruginosa*, which can be quickly and cost-effectively produced[88,89].

Multi-epitope vaccines against *P. aeruginosa* have been studied, but most of them focus on outer membrane protein[90,91]. In this study, we identified 10 proteins reported to protect mice from *P. aeruginosa* infection[12–19]. Also, computational analyses demonstrated that these proteins possessed optimal antigenicity, were non-toxic, and non-allergenic, and lacked a multi-channel transmembrane domain. These strategies allow us to identify the proteins critical for *P. aeruginosa* to survive and contribute to disease, while also reducing the probability of undesirable effects after vaccination. In this way, the designed vaccines have the potential to recognize a variety of antigens, enhancing the immune defense against *P. aeruginosa* and offering a promising strategy to prevent infection.

Both B and T lymphocyte cells are the primary components of the adaptive immune response, collaborating to defend against extrinsic antigens to recognize and eradicate pathogens. To elicit a robust immunological reaction in the host, the vaccines were formulated with a combination of CTL epitopes, HTL epitopes, and B cell epitopes chosen for their antigenicity, immunogenicity, toxicity, and allergenicity. We evaluated the affinity of CTL epitopes and HTL epitopes to MHC molecules. The selected epitopes were appropriately bound to the groove of MHC molecules and able to be detected by the immune system[92]. Additionally, the HBD3 and PorB sequences were used as adjuvant, which was reported to enhance the immune response and promote its durability[53,93].

The physicochemical characteristics of V1 and V2 were assessed, both of which demonstrated non-toxic, non-allergenic, and appropriate antigenicity. The GRAVY and solubility of the vaccines were suitable for the aqueous environment of the host body. The EAAAK, GPGPG, AAY, and KK linkers aided in the proper folding of vaccines and stabilization of their structures. Structural validation of the vaccines was further supported by PROCHECK analysis, with over 90% of the residues falling within the preferred regions on the Ramachandran plot, confirming the rationality and stability of the refined vaccine structures. The vaccines designed in this study suggested a better structural quality than previous studies in this aspect[91,94]. Molecular docking analyses revealed strong binding affinity of both V1 and V2 with TLRs, with HADDOCK scores of -265.5 ± 3.0 and -343.2 ± 5.6 for the V1-TLRs complexes and V2-TLRs complexes. Furthermore, the average RMSD values of V1-TLRs and V2-TLRs complexes were around 1.0 nm during the MD simulation, indicating both of them possessed more stable structure than vaccine alone. The Rg values showed that the V2 and V2-TLRs complex exhibited a tighter structure, while the RMSF analysis demonstrated that V1 was more flexible. Additionally, V1 exhibited a rise in the number of hydrogen bonds, surpassing V2 and showcasing a stronger binding affinity with TLRs. The calculated binding free energy validated that V1 and V2 had a robust binding affinity with TLRs, with V1 performing slightly better. *P. aeruginosa*is usually considered to be an extracellular pathogen that prefers

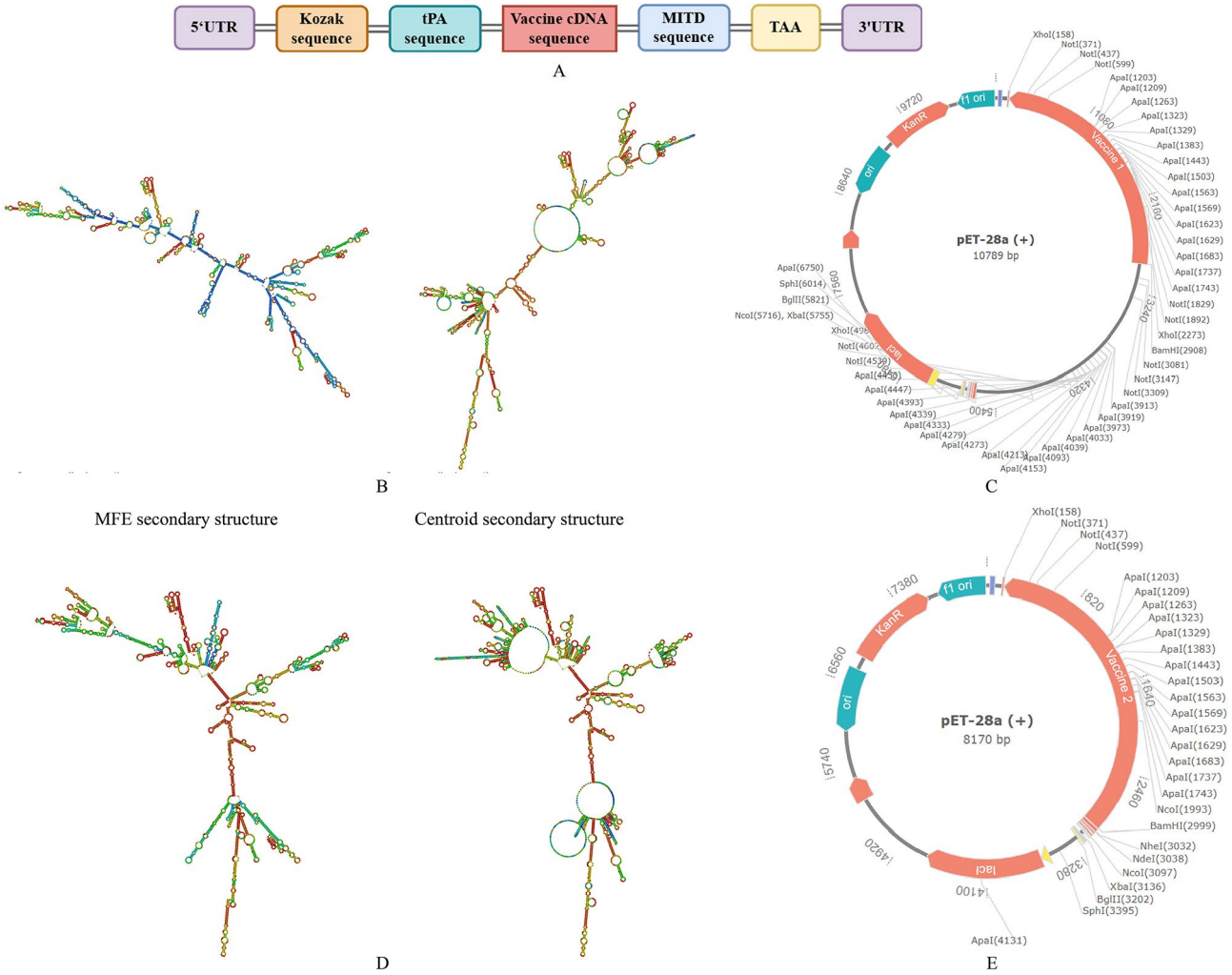

Fig. 8. mRNA Vaccines' structural prediction and expression in pET-28a (+) vector. (**A**) structure of liner RNA; (**B**) The optimal and centroid secondary structure of the V1; (**C**) V1 in the expression vector; (**D**) The optimal and centroid secondary structure of the V2; (E) V2 in the expression vector.

to bind outside host cell membranes and form extracellular biofilms[95]. Importantly, the Immune simulation results suggested that both candidate vaccines induced innate and humoral immune responses, including increased active immune cell populations and high antibody titers, which facilitated host phagocytosis. Also, the candidate vaccines had induced significant cytokines, and the high level of IFN-γ was critical for clearing *P. aeruginosa* infection from the lungs[96]. Moreover, a worldwide population coverage rate (99.30%) of the multi-epitope vaccines indicated their potential utility in a variety of geographical regions. Finally, after optimizing codons and cloning the V1 and V2 sequences into pET-28a (+) of *E. coli* (Strain K12), it was evident that the developed vaccines have promise for future mass manufacturing. This study, based on a computational approach, is theoretically valid, but in vitro and in vivo experiments are needed to verify the effectiveness of the designed vaccines. The accuracy of these predictions may be influenced by incomplete or biased datasets, and the models used may not fully capture the complexity of immune responses in vivo.

Conclusion

Pseudomonas aeruginosa is recognized as an MDR bacterium, featuring a high infection rate, mortality, and healthcare costs among immunocompromised patients. The ultimate objective of this investigation is to design a multi-epitope vaccine utilizing reverse vaccinology and immunoinformatics approaches that will generate a potent and effective immune response in the human body, while also being appropriate for large-scale production in the future. Overall, the results demonstrate that the developed vaccines exhibit the potential to effectively combat *P. aeruginosa* while also being broadly applicable. However, further investigation needs to be conducted to validate the safety and efficacy of these proposed vaccines.

Data availability

The datasets generated and/or analyzed during the current study are available in the article/Supplementary Material. The protein sequences of Type III secretion protein PcrV (UniProt ID: G3XD49), Beta-lactamase (UniProt ID: P24735), B-type flagellin (UniProt ID: P72151), Type IV major pilin protein PilA (UniProt ID: P04739), Fimbrial assembly protein PilQ (UniProt ID: P34750), Translocator protein PopB (UniProt ID: Q9I324), Protein Hcp1 (UniProt ID: Q9I747), Alginate biosynthesis protein (UniProt ID: Q51372), Exotoxin A (UniProt ID: P11439), Chitin-binding protein CbpD (UniProt ID: Q9I589) were retrieved from UniProt Database (https://www.uniprot.org/) and their sequences were listed in supplementary materials. The DNA and mRNA sequences of the designed vaccines were listed in supplementary materials. The GenBank accession numbers of mRNA sequences of the designed vaccines are BankIt2905551 Seq1 PQ773499 (V1) and BankIt2905551 Seq2 PQ773500 (V2).

Received: 11 November 2024; Accepted: 11 February 2025
Published online: 26 March 2025

References

1. Azam, M. W. & Khan, A. U. Updates on the pathogenicity status of Pseudomonas aeruginosa. *Drug Discov Today*. **24**, 350–359. https://doi.org/10.1016/j.drudis.2018.07.003 (2019).
2. Eklöf, J. et al. Pseudomonas aeruginosa and risk of death and exacerbations in patients with chronic obstructive pulmonary disease: an observational cohort study of 22 053 patients. *Clin. Microbiol. Infect.* **26**, 227–234. https://doi.org/10.1016/j.cmi.2019.06.011 (2020).
3. Kollef, M. H. et al. Global prospective epidemiologic and surveillance study of ventilator-associated pneumonia due to Pseudomonas aeruginosa. *Crit. Care Med.* **42**, 2178–2187. https://doi.org/10.1097/CCM.0000000000000510 (2014).
4. Malhotra, S., Hayes, D. & Wozniak, D. J. Cystic fibrosis and Pseudomonas aeruginosa: the host-microbe interface. *Clin. Microbiol. Rev.* **32** https://doi.org/10.1128/CMR.00138-18 (2019).
5. Vidaillac, C. & Chotirmall, S. H. Pseudomonas aeruginosa in bronchiectasis: infection, inflammation, and therapies. *Expert Rev. Respir Med.* **15**, 649–662. https://doi.org/10.1080/17476348.2021.1906225 (2021).
6. Reynolds, D. & Kollef, M. The epidemiology and Pathogenesis and treatment of Pseudomonas aeruginosa infections: an update. *Drugs* **81**, 2117–2131. https://doi.org/10.1007/s40265-021-01635-6 (2021).
7. Eklöf, J. et al. Use of inhaled corticosteroids and risk of acquiring Pseudomonas aeruginosa in patients with chronic obstructive pulmonary disease. *Thorax* **77**, 573–580. https://doi.org/10.1136/thoraxjnl-2021-217160 (2022).
8. Qin, S. et al. Pseudomonas aeruginosa: pathogenesis, virulence factors, antibiotic resistance, interaction with host, technology advances and emerging therapeutics. *Signal. Transduct. Target. Ther.* **7**, 199. https://doi.org/10.1038/s41392-022-01056-1 (2022).
9. Pelegrin, A. C. et al. Pseudomonas aeruginosa: a clinical and genomics update. *FEMS Microbiol. Rev.* **45** https://doi.org/10.1093/femsre/fuab026 (2021).
10. Colque, C. A. et al. Hypermutator Pseudomonas aeruginosa exploits multiple genetic pathways to develop Multidrug Resistance during Long-Term infections in the airways of cystic fibrosis patients. *Antimicrob. Agents Chemother.* **64** https://doi.org/10.1128/AAC.02142-19 (2020).
11. Moxon, R., Reche, P. A., Rappuoli, R. & Editorial Reverse vaccinology. *Front. Immunol.* **10**, 2776. https://doi.org/10.3389/fimmu.2019.02776 (2019).
12. Askarian, F. et al. Immunization with lytic polysaccharide monooxygenase CbpD induces protective immunity against Pseudomonas aeruginosa pneumonia. *Proc. Natl. Acad. Sci. U S A.* **120**, e2301538120. https://doi.org/10.1073/pnas.2301538120 (2023).
13. Bakht Azad, S., Nikokar, I., Faezi, S., Rasooly, S. & Mahdavi, M. Evaluation of the immune responses following co-administration of PilQ and type b-flagellin from Pseudomonas aeruginosa in the burn mouse model. *Microb. Pathog.* **123**, 426–432. https://doi.org/10.1016/j.micpath.2018.07.042 (2018).
14. Campodónico, V. L., Llosa, N. J., Bentancor, L. V., Maira-Litran, T. & Pier, G. B. Efficacy of a conjugate vaccine containing polymannuronic acid and flagellin against experimental Pseudomonas aeruginosa lung infection in mice. *Infect. Immun.* **79**, 3455–3464. https://doi.org/10.1128/IAI.00157-11 (2011).
15. Hashemi, F. B. et al. A trivalent vaccine consisting of flagellin A + B and pilin protects against Pseudomonas aeruginosa infection in a murine burn model. *Microb. Pathog.* **138**, 103697. https://doi.org/10.1016/j.micpath.2019.103697 (2020).
16. Jiang, M., Yao, J. & Feng, G. Protective effect of DNA vaccine encoding pseudomonas exotoxin A and PcrV against acute pulmonary P. aeruginosa infection. *PLoS One.* **9**, e96609. https://doi.org/10.1371/journal.pone.0096609 (2014).
17. Shaikh, M. O. F. et al. Multicomponent Pseudomonas aeruginosa vaccines eliciting Th17 cells and functional antibody responses Confer enhanced Protection against Experimental Acute Pneumonia in mice. *Infect. Immun.* **90**, e0020322. https://doi.org/10.1128/iai.00203-22 (2022).
18. Wang, Y. et al. Development of a chimeric vaccine against Pseudomonas aeruginosa based on the Th17-Stimulating epitopes of PcrV and AmpC. *Front. Immunol.* **11**, 601601. https://doi.org/10.3389/fimmu.2020.601601 (2020).
19. Yang, F. et al. Protective efficacy of the Trivalent Pseudomonas aeruginosa Vaccine candidate PcrV-OprI-Hcp1 in murine pneumonia and burn models. *Sci. Rep.* **7**, 3957. https://doi.org/10.1038/s41598-017-04029-5 (2017).
20. Bowler-Barnett, E. H. et al. UniProt and Mass Spectrometry-based Proteomics-A 2-Way Working Relationship. *Mol. Cell. Proteom.* **22**, 100591. https://doi.org/10.1016/j.mcpro.2023.100591 (2023).
21. Chou, K. C. & Shen, H. B. Cell-PLoc: a package of web servers for predicting subcellular localization of proteins in various organisms. *Nat. Protoc.* **3**, 153–162. https://doi.org/10.1038/nprot.2007.494 (2008).
22. Yu, N. Y. et al. PSORTb 3.0: improved protein subcellular localization prediction with refined localization subcategories and predictive capabilities for all prokaryotes. *Bioinformatics* **26**, 1608–1615. https://doi.org/10.1093/bioinformatics/btq249 (2010).
23. Teufel, F. et al. SignalP 6.0 predicts all five types of signal peptides using protein language models. *Nat. Biotechnol.* **40**, 1023–1025. https://doi.org/10.1038/s41587-021-01156-3 (2022).
24. Ong, E. et al. Vaxign2: the second generation of the first web-based vaccine design program using reverse vaccinology and machine learning. *Nucleic Acids Res.* **49**, W671–W678. https://doi.org/10.1093/nar/gkab279 (2021).
25. Wilkins, M. R. et al. Protein identification and analysis tools in the ExPASy server. *Methods Mol. Biol.* **112**, 531–552 (1999).
26. Reynisson, B., Alvarez, B., Paul, S., Peters, B. & Nielsen, M. NetMHCpan-4.1 and NetMHCIIpan-4.0: improved predictions of MHC antigen presentation by concurrent motif deconvolution and integration of MS MHC eluted ligand data. *Nucleic Acids Res.* **48**, W449–W454. https://doi.org/10.1093/nar/gkaa379 (2020).
27. Alvarez, B. et al. NNAlign_MA; MHC peptidome deconvolution for accurate MHC binding motif characterization and improved T-cell epitope predictions. *Mol. Cell. Proteom.* **18**, 2459–2477. https://doi.org/10.1074/mcp.TIR119.001658 (2019).
28. Vita, R. et al. The Immune Epitope Database (IEDB): 2024 update. *Nucleic Acids Res.* https://doi.org/10.1093/nar/gkae1092 (2024).

29. Doytchinova, I. A. & Flower, D. R. VaxiJen: a server for prediction of protective antigens, tumour antigens and subunit vaccines. *BMC Bioinform.* **8**, 4 (2007).
30. Dimitrov, I., Bangov, I., Flower, D. R. & Doytchinova, I. AllerTOP v.2–a server for in silico prediction of allergens. *J. Mol. Model.* **20**, 2278. https://doi.org/10.1007/s00894-014-2278-5 (2014).
31. Rathore, A. S., Choudhury, S., Arora, A., Tijare, P. & Raghava, G. P. ToxinPred 3.0: an improved method for predicting the toxicity of peptides. *Comput. Biol. Med.* **179**, 108926. https://doi.org/10.1016/j.compbiomed.2024.108926 (2024).
32. Fleri, W. et al. The Immune Epitope Database and Analysis Resource in Epitope Discovery and Synthetic Vaccine Design. *Front. Immunol.* **8**, 278. https://doi.org/10.3389/fimmu.2017.00278 (2017).
33. Aune, T. M., Penix, L. A., Rincón, M. R. & Flavell, R. A. Differential transcription directed by discrete gamma interferon promoter elements in naive and memory (effector) CD4 T cells and CD8 T cells. *Mol. Cell. Biol.* **17**, 199–208 (1997).
34. Gandhi, N. A. et al. Targeting key proximal drivers of type 2 inflammation in disease. *Nat. Rev. Drug Discov.* **15**, 35–50. https://doi.org/10.1038/nrd4624 (2016).
35. Dhanda, S. K., Gupta, S., Vir, P. & Raghava, G. P. S. Prediction of IL4 inducing peptides. *Clin. Dev. Immunol.* **2013** (263952). https://doi.org/10.1155/2013/263952 (2013).
36. Dhanda, S. K., Vir, P. & Raghava, G. P. S. Designing of interferon-gamma inducing MHC class-II binders. *Biol. Direct.* **8**, 30. https://doi.org/10.1186/1745-6150-8-30 (2013).
37. Protein Data Bank. The single global archive for 3D macromolecular structure data. *Nucleic Acids Res.* **47**, D520–D528. https://doi.org/10.1093/nar/gky949 (2019).
38. Waterhouse, A. et al. SWISS-MODEL: homology modelling of protein structures and complexes. *Nucleic Acids Res.* **46**, W296–W303. https://doi.org/10.1093/nar/gky427 (2018).
39. Kurcinski, M., Badaczewska-Dawid, A., Kolinski, M., Kolinski, A. & Kmiecik, S. Flexible docking of peptides to proteins using CABS-dock. *Protein Sci.* **29**, 211–222. https://doi.org/10.1002/pro.3771 (2020).
40. Rosignoli, S. & Paiardini, A. Boosting the full potential of PyMOL with Structural Biology Plugins. *Biomolecules* **12** https://doi.org/10.3390/biom12121764 (2022).
41. Saha, S. & Raghava, G. P. S. Prediction of continuous B-cell epitopes in an antigen using recurrent neural network. *Proteins* **65**, 40–48 (2006).
42. Saha, S. & Raghava, G. P. S. Prediction methods for B-cell epitopes. *Methods Mol. Biol.* **409**, 387–394. https://doi.org/10.1007/978-1-60327-118-9_29 (2007).
43. Bui, H. H., Sidney, J., Li, W., Fusseder, N. & Sette, A. Development of an epitope conservancy analysis tool to facilitate the design of epitope-based diagnostics and vaccines. *BMC Bioinform.* **8**, 361 (2007).
44. Ahmad, S. et al. In silico design of a novel multi-epitope vaccine against HCV infection through immunoinformatics approaches. *Int. J. Biol. Macromol.* **267**, 131517. https://doi.org/10.1016/j.ijbiomac.2024.131517 (2024).
45. Kar, T. et al. A candidate multi-epitope vaccine against SARS-CoV-2. *Sci. Rep.* **10**, 10895. https://doi.org/10.1038/s41598-020-67749-1 (2020).
46. Aldakheel, F. M. et al. Proteome-wide mapping and reverse vaccinology approaches to design a Multi-epitope Vaccine against Clostridium perfringens. *Vaccines (Basel).* **9** https://doi.org/10.3390/vaccines9101079 (2021).
47. Obaidullah, A. J. et al. Immunoinformatics-guided design of a multi-epitope vaccine based on the structural proteins of severe acute respiratory syndrome coronavirus 2. *RSC Adv.* **11**, 18103–18121. https://doi.org/10.1039/d1ra02885e (2021).
48. Batoni, G., Maisetta, G., Esin, S. & Campa, M. Human beta-defensin-3: a promising antimicrobial peptide. *Mini Rev. Med. Chem.* **6**, 1063–1073 (2006).
49. Lisk, C. et al. Toll-like receptor ligand based adjuvant, PorB, Increases Antigen Deposition on Germinal Center Follicular dendritic cells while enhancing the follicular dendritic cells network. *Front. Immunol.* **11**, 1254. https://doi.org/10.3389/fimmu.2020.01254 (2020).
50. Tewary, P. et al. β-Defensin 2 and 3 promote the uptake of self or CpG DNA, enhance IFN-α production by human plasmacytoid dendritic cells, and promote inflammation. *J. Immunol.* **191**, 865–874. https://doi.org/10.4049/jimmunol.1201648 (2013).
51. Mosaheb, M. & Wetzler, L. M. Meningococcal PorB induces a robust and diverse antigen specific T cell response as a vaccine adjuvant. *Vaccine* **36**, 7689–7699. https://doi.org/10.1016/j.vaccine.2018.10.074 (2018).
52. Liu, X., Wetzler, L. M. & Massari, P. The PorB porin from commensal Neisseria lactamica induces Th1 and Th2 immune responses to ovalbumin in mice and is a potential immune adjuvant. *Vaccine* **26**, 786–796. https://doi.org/10.1016/j.vaccine.2007.11.080 (2008).
53. Alexander, J. et al. Development of experimental carbohydrate-conjugate vaccines composed of Streptococcus pneumoniae capsular polysaccharides and the universal helper T-lymphocyte epitope (PADRE). *Vaccine* **22**, 2362–2367 (2004).
54. Li, G. et al. Construction of a linker library with widely controllable flexibility for fusion protein design. *Appl. Microbiol. Biotechnol.* **100**, 215–225. https://doi.org/10.1007/s00253-015-6985-3 (2016).
55. Ullah, A. et al. An in Silico multi-epitopes Vaccine Ensemble and characterization against nosocomial Proteus penneri. *Mol. Biotechnol.* **66**, 3498–3513. https://doi.org/10.1007/s12033-023-00949-y (2024).
56. Buchan, D. W. A. & Jones, D. T. The PSIPRED Protein Analysis Workbench: 20 years on. *Nucleic Acids Res.* **47**, W402–W407. https://doi.org/10.1093/nar/gkz297 (2019).
57. Kim, D. E., Chivian, D. & Baker, D. Protein structure prediction and analysis using the Robetta server. *Nucleic Acids Res.* **32**, W526–W531 (2004).
58. Bhattacharya, D., Nowotny, J., Cao, R. & Cheng, J. 3Drefine: an interactive web server for efficient protein structure refinement. *Nucleic Acids Res.* **44**, W406–W409. https://doi.org/10.1093/nar/gkw336 (2016).
59. Colovos, C. & Yeates, T. O. Verification of protein structures: patterns of nonbonded atomic interactions. *Protein Sci.* **2**, 1511–1519 (1993).
60. Wiederstein, M. & Sippl, M. J. ProSA-web: interactive web service for the recognition of errors in three-dimensional structures of proteins. *Nucleic Acids Res.* **35**, W407–W410 (2007).
61. Jespersen, M. C., Peters, B., Nielsen, M. & Marcatili, P. BepiPred-2.0: improving sequence-based B-cell epitope prediction using conformational epitopes. *Nucleic Acids Res.* **45**, W24–W29. https://doi.org/10.1093/nar/gkx346 (2017).
62. Sun, P. et al. Bioinformatics resources and tools for conformational B-cell epitope prediction. *Computational and Mathematical Methods In Medicine* 943636, (2013). https://doi.org/10.1155/2013/943636 (2013).
63. Ponomarenko, J. et al. ElliPro: a new structure-based tool for the prediction of antibody epitopes. *BMC Bioinform.* **9**, 514. https://doi.org/10.1186/1471-2105-9-514 (2008).
64. Cia, G., Pucci, F. & Rooman, M. Critical review of conformational B-cell epitope prediction methods. *Brief. Bioinform.* **24** https://doi.org/10.1093/bib/bbac567 (2023).
65. Medzhitov, R. Toll-like receptors and innate immunity. *Nat. Rev. Immunol.* **1**, 135–145 (2001).
66. Kozakov, D. et al. The ClusPro web server for protein-protein docking. *Nat. Protoc.* **12**, 255–278. https://doi.org/10.1038/nprot.2016.169 (2017).
67. van Zundert, G. C. P. et al. The HADDOCK2.2 web server: user-friendly integrative modeling of Biomolecular complexes. *J. Mol. Biol.* **428**, 720–725. https://doi.org/10.1016/j.jmb.2015.09.014 (2016).
68. Laskowski, R. A. et al. Structural summaries of PDB entries. *Protein Sci.* **27**, 129–134. https://doi.org/10.1002/pro.3289 (2018).
69. Abraham, M. J. et al. High performance molecular simulations through multi-level parallelism from laptops to supercomputers. *SoftwareX 1–2.* **GROMACS**, 19–25. https://doi.org/10.1016/j.softx.2015.06.001 (2015).

70. Smith, M. D., Rao, J. S., Segelken, E. & Cruz, L. Force-Field induced bias in the structure of Aβ21-30: A comparison of OPLS, AMBER, CHARMM, and GROMOS force fields. *J. Chem. Inf. Model* **55**, 2587–2595. https://doi.org/10.1021/acs.jcim.5b00308 (2015).
71. Valdés-Tresanco, M. S., Valdés-Tresanco, M. E., Valiente, P. A., Moreno, E. & gmx_MMPBSA A New Tool to perform end-state Free Energy calculations with GROMACS. *J. Chem. Theory Comput.* **17**, 6281–6291. https://doi.org/10.1021/acs.jctc.1c00645 (2021).
72. Rapin, N., Lund, O., Bernaschi, M. & Castiglione, F. Computational immunology meets bioinformatics: the use of prediction tools for molecular binding in the simulation of the immune system. *PLoS One*. **5**, e9862. https://doi.org/10.1371/journal.pone.0009862 (2010).
73. Stolfi, P. et al. In-silico evaluation of adenoviral COVID-19 vaccination protocols: Assessment of immunological memory up to 6 months after the third dose. *Front. Immunol.* **13**, 998262. https://doi.org/10.3389/fimmu.2022.998262 (2022).
74. Payne, R. P. et al. Immunogenicity of standard and extended dosing intervals of BNT162b2 mRNA vaccine. *Cell* **184** https://doi.org/10.1016/j.cell.2021.10.011 (2021).
75. Bui, H. H. et al. Predicting population coverage of T-cell epitope-based diagnostics and vaccines. *BMC Bioinform.* **7**, 153 (2006).
76. Craig, D. B. & Dombkowski, A. A. Disulfide by Design 2.0: a web-based tool for disulfide engineering in proteins. *BMC Bioinform.* **14**, 346. https://doi.org/10.1186/1471-2105-14-346 (2013).
77. Olson, S. A. EMBOSS opens up sequence analysis. European Molecular Biology Open Software suite. *Brief. Bioinform*. **3**, 87–91 (2002).
78. Grote, A. et al. JCat: a novel tool to adapt codon usage of a target gene to its potential expression host. *Nucleic Acids Res.* **33**, W526–W531 (2005).
79. Sharp, P. M. & Li, W. H. The codon Adaptation Index–a measure of directional synonymous codon usage bias, and its potential applications. *Nucleic Acids Res.* **15**, 1281–1295 (1987).
80. Ramalingam, P. S. & Arumugam, S. Reverse vaccinology and immunoinformatics approaches to design multi-epitope based vaccine against oncogenic KRAS. *Med. Oncol.* **40**, 283. https://doi.org/10.1007/s12032-023-02160-0 (2023).
81. Gruber, A. R., Lorenz, R., Bernhart, S. H., Neuböck, R. & Hofacker, I. L. The Vienna RNA websuite. *Nucleic Acids Res.* **36**, W70–W74. https://doi.org/10.1093/nar/gkn188 (2008).
82. Stanislavsky, E. S. & Lam, J. S. Pseudomonas aeruginosa antigens as potential vaccines. *FEMS Microbiol. Rev.* **21**, 243–277 (1997).
83. Lyczak, J. B., Cannon, C. L. & Pier, G. B. Lung infections associated with cystic fibrosis. *Clin. Microbiol. Rev.* **15**, 194–222 (2002).
84. Murphy, T. F. Pseudomonas aeruginosa in adults with chronic obstructive pulmonary disease. *Curr. Opin. Pulm Med.* **15**, 138–142. https://doi.org/10.1097/MCP.0b013e328321861a (2009).
85. Breidenstein, E. B. M., de la Fuente-Núñez, C. & Hancock, R. E. W. Pseudomonas aeruginosa: all roads lead to resistance. *Trends Microbiol.* **19**, 419–426. https://doi.org/10.1016/j.tim.2011.04.005 (2011).
86. Daikos, G. L. et al. Review of Ceftazidime-Avibactam for the treatment of infections caused by Pseudomonas aeruginosa. *Antibiot. (Basel)*. **10** https://doi.org/10.3390/antibiotics10091126 (2021).
87. Tenover, F. C., Nicolau, D. P. & Gill, C. M. Carbapenemase-producing Pseudomonas aeruginosa -an emerging challenge. *Emerg. Microbes Infect.* **11**, 811–814. https://doi.org/10.1080/22221751.2022.2048972 (2022).
88. Mora, M., Veggi, D., Santini, L., Pizza, M. & Rappuoli, R. Reverse vaccinology. *Drug Discov Today*. **8**, 459–464 (2003).
89. De Groot, A. S. et al. Better Epitope Discovery, Precision Immune Engineering, and accelerated Vaccine Design using Immunoinformatics Tools. *Front. Immunol.* **11**, 442. https://doi.org/10.3389/fimmu.2020.00442 (2020).
90. Kalantari, H., Habibi, M., Ferdousi, A., Asadi Karam, M. R. & Mohammadian, T. Development of a multi-epitope vaccine candidate against Pseudomonas aeruginosa causing urinary tract infection and evaluation of its immunoreactivity in a rabbit model. *J. Biomol. Struct. Dyn.* **42**, 6212–6227. https://doi.org/10.1080/07391102.2023.2239915 (2024).
91. Roy, S. K. et al. A computational approach to developing a multi-epitope vaccine for combating Pseudomonas aeruginosa-induced pneumonia and sepsis. *Brief. Bioinform.* **25** https://doi.org/10.1093/bib/bbae401 (2024).
92. Sagert, L., Hennig, F., Thomas, C. & Tampé, R. A loop structure allows TAPBPR to exert its dual function as MHC I chaperone and peptide editor. *Elife* **9** https://doi.org/10.7554/eLife.55326 (2020).
93. Kim, J., Yang, Y. L., Jang, S. H. & Jang, Y. S. Human β-defensin 2 plays a regulatory role in innate antiviral immunity and is capable of potentiating the induction of antigen-specific immunity. *Virol. J.* **15**, 124. https://doi.org/10.1186/s12985-018-1035-2 (2018).
94. Asadinezhad, M. et al. Development of innovative multi-epitope mRNA vaccine against Pseudomonas aeruginosa using in silico approaches. *Brief. Bioinform.* **25** https://doi.org/10.1093/bib/bbad502 (2023).
95. Lovewell, R. R., Patankar, Y. R. & Berwin, B. Mechanisms of phagocytosis and host clearance of Pseudomonas aeruginosa. *Am. J. Physiol. Lung Cell. Mol. Physiol.* **306**, L591–L603. https://doi.org/10.1152/ajplung.00335.2013 (2014).
96. Krause, A. et al. Protective anti-pseudomonas aeruginosa humoral and cellular mucosal immunity by AdC7-mediated expression of the P. aeruginosa protein OprF. *Vaccine* **29**, 2131–2139. https://doi.org/10.1016/j.vaccine.2010.12.087 (2011).

Acknowledgements

The following sources provided support for this investigation: the Natural Science Foundation of Changsha (No. kq2208368); the National Natural Science Foundation of China (No. 81770080); the National Natural Science Foundation of China (No. 8210012334); the Key R&D Program of Hunan Province (No. 2022SK2038); the Natural Science Foundation of Hunan Province of China (No.2023JJ30930); the Scientific Research Program of FuRong Laboratory (No.2023SK2101); the national key clinical specialist construction programs of China (Grant Number z047-02); the Research Project of Teaching Reform in Colleges and Universities in Hunan Province (2021jy139-2); the China Postdoctoral Science Foundation (2022M713520); the Research Project on teaching reform of ordinary colleges and universities in Hunan province (2022JGYB037), and the Project Program of central south university graduate education teaching reform (No. 2022JGB025); the National Natural Science Foundation of China (grant number 82470078).

Author contributions

FZ: Conceptualization, Methodology, Writing- Reviewing and Editing. RQ: Data curation, Writing- Original draft preparation. SM and ZZ: Resources, Investigation. CT: Visualization. HY: Supervision. PZ and YX: Validation. YL: Formal analysis. JC and PP: Project administration, Funding acquisition.

Declarations

Competing interests

The authors declare no competing interests.

Additional information

Supplementary Information The online version contains supplementary material available at https://doi.org/10.1038/s41598-025-90226-6.

Correspondence and requests for materials should be addressed to J.C. or P.P.

Reprints and permissions information is available at www.nature.com/reprints.

Publisher's note Springer Nature remains neutral with regard to jurisdictional claims in published maps and institutional affiliations.